Cleaner Extraction of Lead from Complex Lead-Containing Wastes by Reductive Sulfur-Fixing Smelting with Low SO$_2$ Emission

Yun Li [1,2], Shenghai Yang [1], Wenrong Lin [1,3], Pekka Taskinen [2], Jing He [1], Yuejun Wang [4], Junjie Shi [2], Yongming Chen [1,*], Chaobo Tang [1,*] and Ari Jokilaakso [1,2,*]

[1] School of Metallurgy and Environment, Central South University, Changsha 410083, China;
yun.li@aalto.fi (Y.L.); yangshcsu@163.com (S.Y.); linwenrong@zh-coslight.com (W.L.); he6213@163.com (J.H.)

[2] Department of Chemical and Metallurgical Engineering, School of Chemical Engineering, Aalto University,
02150 Espoo, Finland; pekka.taskinen@aalto.fi (P.T.); junjie.shi@aalto.fi (J.S.)

[3] Zhuhai Coslight Battery Co., Ltd, Zhuhai 519180, China

[4] Department of Ecology and Resources Engineering, Hetao College, Bayannur 015000, China;
thirtythree61@aliyun.com

* Correspondence: csuchenyongming@163.com (Y.C.); chaobotang@163.com (C.T.);
ari.jokilaakso@aalto.fi (A.J.); Tel.: +86-731-88830470 (Y.C. & C.T.); +358-50-3138885 (A.J.)

check for updates

Abstract: A novel and cleaner process for lead and silver recycling from multiple lead-containing wastes, e.g., lead ash, lead sludge, lead slag, and ferric sludge, by reductive sulfur-fixing smelting was proposed. In this process, coke and iron-containing wastes were employed as reductive agent and sulfur-fixing agent, respectively. A Na$_2$CO$_3$-Na$_2$SO$_4$ mixture was added as flux. The feasibility of this process was detected from thermodynamic and experimental perspectives. The influence of Fe/SiO$_2$ and CaO/SiO$_2$, composition of the molten salt, coke addition, smelting temperature, and smelting time on direct Pb recovery and sulfur-fixation efficiency were investigated. The optimal process conditions were determined as follows: W_{Coke} = 15% $W_{\mathrm{Pb\ wastes}}$, $W_{\mathrm{Na_2CO_3}}/W_{\mathrm{Na_2SO_4}}$ = 0.7/0.3, Fe/SiO$_2$ = 1.10, CaO/SiO$_2$ = 0.30, smelting temperature 1200 °C, and smelting time 2 h, where W represents weight. Under these optimum conditions, 92.4% Pb and 98.8% Ag were directly recovered in crude lead bullion in one step treatment, and total 98.6% sulfur was fixed. The generation and emissions of SO$_2$ can be avoided. The main phases in ferrous matte obtained were FeS, NaFeS$_2$, Fe$_2$Zn$_3$S$_5$, and a little entrained Pb. The slag was a FeO-SiO$_2$-CaO-Na$_2$O quaternary melt.

Keywords: SO$_2$-free sulfur fixing smelting; lead recycling; wastes co-treatment and recycling; lead-iron-containing wastes; molten salt; PbO-FeO-SiO$_2$-CaO-Na$_2$O phase diagram

1. Introduction

Today, large amounts of lead-containing wastes are produced in non-ferrous metallurgical industry [1–3], especially in Pb and Zn metallurgy fields, such as lead ash and lead slag generated in Pb/Zn smelting, lead anode slime, and lead sludge produced in the electrolytic refining. Other engineering fields [4–6] are also sources of Pb-bearing substances, including lead scrap and lead paste separated from spent lead-acid batteries [7]. In many countries, these lead-bearing wastes are classified as hazardous waste due to the high toxicity of lead [8]. They are greatly detrimental to environment and human health if left untreated and abandoned directly to the environment [9,10]. However, these wastes generally contain considerable amounts of precious metals, such as gold (Au) and silver (Ag). It also enormously challenges the circular economy if the valuable metals are not recycled. Various lead wastes are potential resources for extracting lead and precious metals

considering the fact that the grades of lead concentrates are decreasing [11] and primary lead ores are gradually exhausting.

Many studies about the treatment of Pb-containing wastes using pyrometallurgical and hydrometallurgical processes were reported in recent years [12,13]. The immobilization of lead slags to prepare construction materials and inorganic polymers were also investigated [14,15]. Hydrometallurgical methods also can be applied for various Pb-bearing wastes treatment. They often consist of a two-step process of leaching and separation in acid [16], alkaline [17], and other lixiviants [18,19]. Many hydrometallurgical processes involve shortcomings of a long process chain, large amounts of reagents consumption, and waste water generation. Most hydrometallurgical disposal processes of lead wastes are still far from the industrial production scale.

Pyrometallurgy is the predominant methodology around the world for primary lead production. Reverberatory smelting and bath smelting are the two main technologies [20]. Generally, sulfur content in the feed required in the reverberatory smelting techniques is lower than 2%. As a result, SO_2 emission is inevitable with Pb-bearing wastes because sulfur contents of lead wastes typically are higher than 2%. Thus, a high energy consumption and heavy pollution are involved when using the reverberatory smelting technology. At present, many lead and zinc smelters apply bath smelting processes to treat Pb wastes along with the primary raw materials [21], such as spent lead-acid battery pastes, lead slags, and other ferrous wastes. However, compared to the primary sulfide concentrate, the sulfur content in wastes is too low to provide enough heat for the smelting when considering the endothermic decomposition reactions of sulfate [22]. Therefore, the use of waste materials often leads to an unstable smelting operation. Moreover, some new technologies [23–25] such as vacuum separation have been reported to treat lead-bearing residues and lead paste. They need a desulfurization pre-treatment step, and the operation cost is relatively high.

Alkaline smelting was first employed by researchers of the former Soviet Union to extract lead from lead sulfide using molten NaOH [26]. Subsequently, more molten salt systems were further developed and introduced to extract lead [27], antimony [28], and bismuth [29] due to the high solvent property, thermal stability, and electrical property of molten salt [30]. In the molten salt smelting, the traditional FeO-SiO_2-CaO slag will be replaced by a molten salt.

In view of environment protection and comprehensive utilization of secondary resources, this investigation proposed a promising new process, referred to as reducing sulfur-fixing smelting, to efficiently recover Pb, Ag and recycle iron and sulfur values from lead-bearing wastes in an environmentally friendly manner. Na_2CO_3-Na_2SO_4 binary salt was used as reaction medium. The novelty of this process is treatment of various iron-lead-bearing wastes, SO_2-free sulfur fixation, a much shorter flowsheet, absence of harmful by-product, and a wide adaptability for different secondary materials. This work investigated the experimental feasibility of this new process in detail. The effects of slag property, feed mixture of different raw materials, and smelting temperature and time on lead recovery and sulfur-fixation efficiency were determined. Furthermore, a series of bench-pilot experiments were conducted. The distributions of Pb, Fe, and S were also evaluated.

2. Experimental

2.1. Materials

The lead-bearing wastes used in this study come from the processes of Chinese metallurgical industry. The feed mixture contained lead ash, lead sludge, lead slag, and ferric sludge. In order to have a steady assay of the feed, 23.9 g lead ash, 48.0 g lead sludge, 5.0 g lead slag, and 23.1 g ferric sludge were manually and carefully mixed to obtain a mixture containing 30% of Pb and 8% of S. Coke used as the reducing agent in this research had fixed carbon of 84.3%. The chemical compositions of the materials are given in Table 1. Figure 1 illustrates the X-ray diffraction analysis results (XRD, D/max 2550PC, Rigaku Co. Ltd, Tokyo, Japan). Other reagents, including Na_2CO_3 and Na_2SO_4, flux Fe_2O_3, SiO_2, and CaO, were analytical purity and supplied by Aladdin Industrial Corporation, China.

Table 1. Chemical compositions of the materials and their mixture (wt.%).

Materials	Pb	S	Fe	Zn	Ag *	SiO$_2$	CaO
Lead ash	49.08	6.74	3.78	2.22	45	0.89	0.39
Lead sludge	30.51	12.19	3.77	6.72	65	5.93	8.61
Lead slag	18.56	0.72	8.89	0.42	35	44.13	0.79
Iron sludge	11.61	2.17	40.07	0.36	730	6.84	7.83
Mixture	30.00	8.00	12.41	4.2	236	7.19	6.07

	Industrial Analysis/%			Chemical Composiztion of the Ash/%			
Coke	C$_{fix}$ *	V$_d$ *	A$_d$ *	Fe$_{total}$	SiO$_2$	CaO	Al$_2$O$_3$
	81.27	3.30	15.43	25.23	41.23	6.60	25.24

* g/t; C$_{fix}$: fixed carbon; V$_d$: dry basis volatiles; A$_d$: dry basis ash.

Figure 1. XRD patterns of the feed materials.

The XRD spectra shows that the main lead-bearing phases in the feed materials were sulfate (PbSO$_4$), sulfide (PbS), oxide (Pb$_3$O$_4$ and PbO$_2$), and silicate (PbSiO$_3$). At the same time, zinc sulfate (ZnSO$_4$), zinc oxysulfate (Zn$_3$O(SO$_4$)$_2$), iron sulfate (Fe$_2$(SO$_4$)$_3$), calcium sulfate (CaSO$_4$), a complex lead-zinc mineral queitite (Pb$_4$Zn$_2$((SO$_4$)(SiO$_4$)(Si$_2$O$_7$)), iron silicate (FeSiO$_3$), and ferric oxide (Fe$_2$O$_3$) were also detected in the materials. The feed material is thus a polymetallic complex material.

2.2. Methods

Figure 2 shows a detailed flowchart of this novel process. As an experimental procedure, 100 g lead-bearing waste mixture was mixed with coke powder, Na_2CO_3-Na_2SO_4 mixture, and other fluxes (CaO, SiO_2 and Fe_2O_3 if necessary). The mixture was placed in an alumina crucible. The crucible was pushed into the constant temperature zone of a tube furnace at the desired temperature. The schematic of the tube furnace is illustrated in Figure 3. In the smelting process, a series of reduction and sulfur-fixation reactions took place between the reactants. Metallic Pb was extracted from the raw materials and enriched in crude lead bullion. At the same time, the sulfur was fixed as ferrous matte, instead of emitting SO_2. After the required smelting time in air, the crucible was taken out from the hot zone and cooled to room temperature. Next, the crucible was broken to carefully separate and weigh the smelting products obtained, crude lead, ferrous matte, and slag. The products were analyzed by Inductively Coupled Plasma-Atomic Emission Spectrometry (ICP-AES, Optima 3000, Perkin Elmer, Norwalk, CT, USA) and X-ray diffractometer.
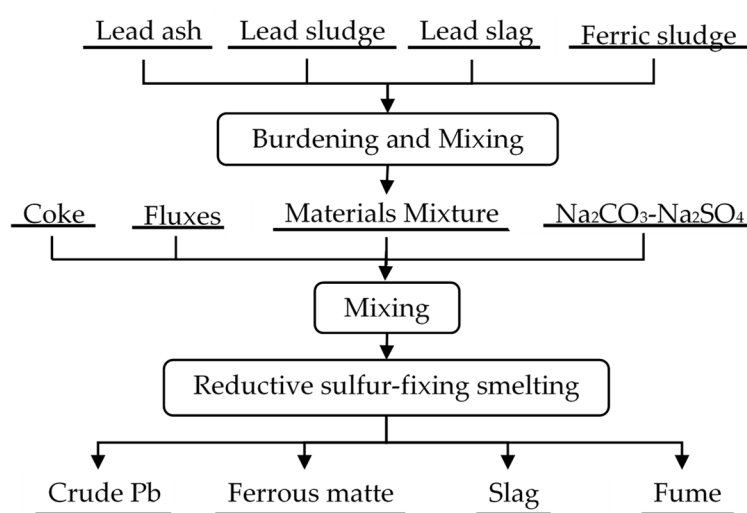
Figure 2. Process flow chart of the reductive sulfur-fixing smelting.
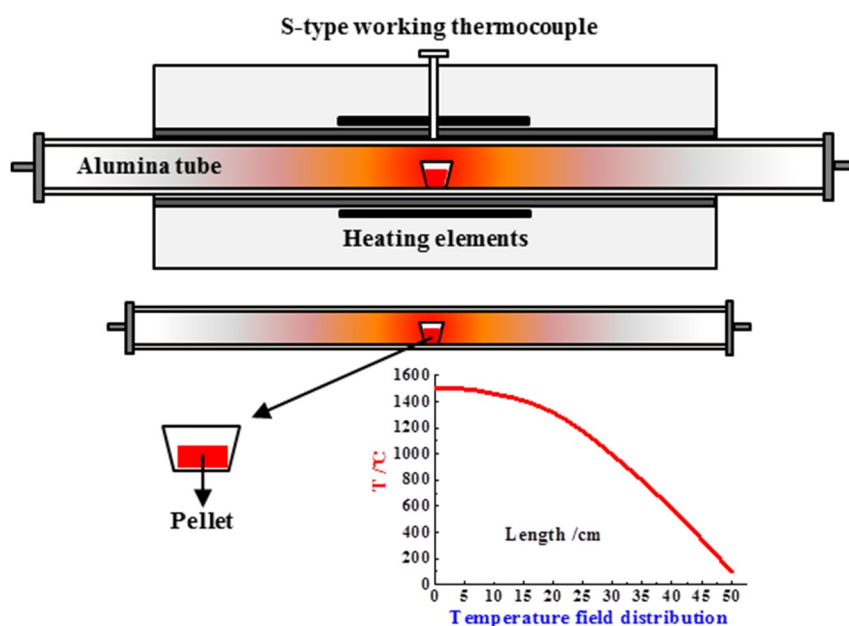
Figure 3. A schematic of the experimental apparatus.

The direct Pb recovery η and sulfur-fixing rate ξ were calculated using the following equations:

$$\text{Direct Pb recovery } \eta \; = \; \frac{\text{Mass of lead in the crude lead}}{\text{Mass of lead in the initial feed materials}} \tag{1}$$

$$\text{Sulfur} - \text{fixation rate } \xi = \frac{\text{Mass of sulfur in the matte and slag}}{\text{Mass of sulfur in the initial feed materials}} \tag{2}$$

3. Thermodynamics Consideration

The main lead-bearing phases in the feed materials are lead sulfate ($PbSO_4$), lead sulfide (PbS), and lead oxide (PbO). In the smelting process, a series of reduction and sulfur-fixation reactions took place between the reactants at high temperature (1000–1300 °C), as shows in Table 2.

Table 2. Possible reactions taking place in the reductive sulfur-fixing smelting process of lead-bearing complex mixture.

Reactions	$\Delta G_T^\theta - T$ [kJ/mol,°C] [31]	Equation
$3Fe_2O_3 + C = 2Fe_3O_4 + CO(g)$	$\Delta G_T^\theta = -0.235\,T + 74.482$	(3)
$3Fe_2O_3 + CO(g) = Fe_3O_4 + CO_2(g)$	$\Delta G_T^\theta = -0.061\,T - 47.13$	(4)
$3/16\,PbSO_4 + 1/16\,Fe_3O_4 + C = 3/16\,Pb + 3/16\,FeS + CO(g)$	$\Delta G_T^\theta = -0.177\,T + 61.90$	(5)
$3/16\,PbSO_4 + 1/16\,Fe_3O_4 + CO(g) = 3/16\,Pb + 3/16\,FeS + CO_2(g)$	$\Delta G_T^\theta = -0.004\,T - 60.39$ $T \le 860\,°C$ $\Delta G_T^\theta = 0.004\,T - 67.22$ $T \ge 860\,°C$	(6)
$3/4\,PbS + 1/4\,Fe_3O_4 + C = 3/4\,Pb + 3/4\,FeS + CO(g)$	$\Delta G_T^\theta = -0.192\,T + 117.48$	(7)
$3/4\,PbS + 1/4\,Fe_3O_4 + CO(g) = 3/4\,Pb + 3/4\,FeS + CO_2(g)$	$\Delta G_T^\theta = -0.017\,T - 5.932$	(8)
$1/5\,PbSO_4 + 1/5\,ZnO + C = 1/5\,Pb + 1/5\,ZnS + CO(g)$	$\Delta G_T^\theta = -0.172\,T + 51.4$	(9)
$1/5\,PbSO_4 + 1/5\,ZnO + CO(g) = 1/5\,Pb + 1/5\,ZnS + CO_2(g)$	$\Delta G_T^\theta = -0.004\,T - 353.56$ $T \le 900\,°C$ $\Delta G_T^\theta = -0.0096\,T - 79.87$ $T \ge 900\,°C$	(10)
$PbS + ZnO + C = Pb + ZnS + CO(g)$	$\Delta G_T^\theta = -0.177\,T + 83.51$	(11)
$PbS + ZnO + CO(g) = Pb + ZnS + CO_2(g)$	$\Delta G_T^\theta = -0.007\,T - 37.229$ $T \le 1100\,°C$ $\Delta G_T^\theta = -0.031\,T - 79.884$ $T \ge 1100\,°C$	(12)
$1/6\,PbSO_4 + 1/6\,Na_2CO_3 + C = 1/6\,Pb + 1/6\,Na_2S + 7/6\,CO(g)$	$\Delta G_T^\theta = -0.196\,T + 92.02$	(13)
$1/5\,PbSO_4 + 1/5\,Na_2CO_3 + CO(g) = 1/5\,Pb + 1/5\,Na_2S + 6/5\,CO_2(g)$	$\Delta G_T^\theta = -0.025\,T - 37.68$	(14)
$1/2\,PbS + 1/2\,Na_2CO_3 + C = 1/2\,Pb + 1/2\,Na_2S + 3/2\,CO(g)$	$\Delta G_T^\theta = -0.244\,T + 189.31$	(15)
$PbS + Na_2CO_3 + CO(g) = Pb + Na_2S + 2CO_2(g)$	$\Delta G_T^\theta = -0.138\,T + 131.78$	(16)
$2/7\,Na_2SO_4 + 2/7\,FeS + C = 2/7\,NaFeS_2 + 1/7\,Na_2O + CO(g)$	$\Delta G_T^\theta = -0.150\,T + 107.28$	(17)
$2/7\,Na_2SO_4 + 2/7\,FeS + CO(g) = 2/7\,NaFeS_2 + 1/7\,Na_2O + CO_2(g)$	$\Delta G_T^\theta = 0.025\,T - 16.13$	(18)
$PbO + C = Pb + CO(g)$	$\Delta G_T^\theta = -0.178\,T + 51.425$	(19)
$PbO + CO(g) = Pb + CO_2(g)$	$\Delta G_T^\theta = -0.112\,T - 67.781$ $T \le 880\,°C$ $\Delta G_T^\theta = 0.014\,T - 91.033$ $T \ge 880\,°C$	(20)

The Gibbs energy change ΔG_T^θ of all above reactions was calculated using HSC Chemistry 9.2.6 and its database [31]. Figure 4 shows the ΔG_T^θ vs.T diagrams of Reactions (3)–(20). It illustrates that lead extraction reactions in the presence of sulfur-fixing agents and reductant are thermodynamically favorable in the temperature range of 900–1300 °C. Increase in temperature will promote the positive trends of the reactions. The reductive sulfur-fixing reactions in this smelting process are feasible. Metallic Pb can be extracted from $PbSO_4$, PbS, and PbO, and enriched in crude lead bullion. At the

same time, the sulfur in the initial raw materials was transferred to FeS, NaFeS$_2$, ZnS, and ultimately fixed as ferrous matte, instead of emitting SO$_2$.
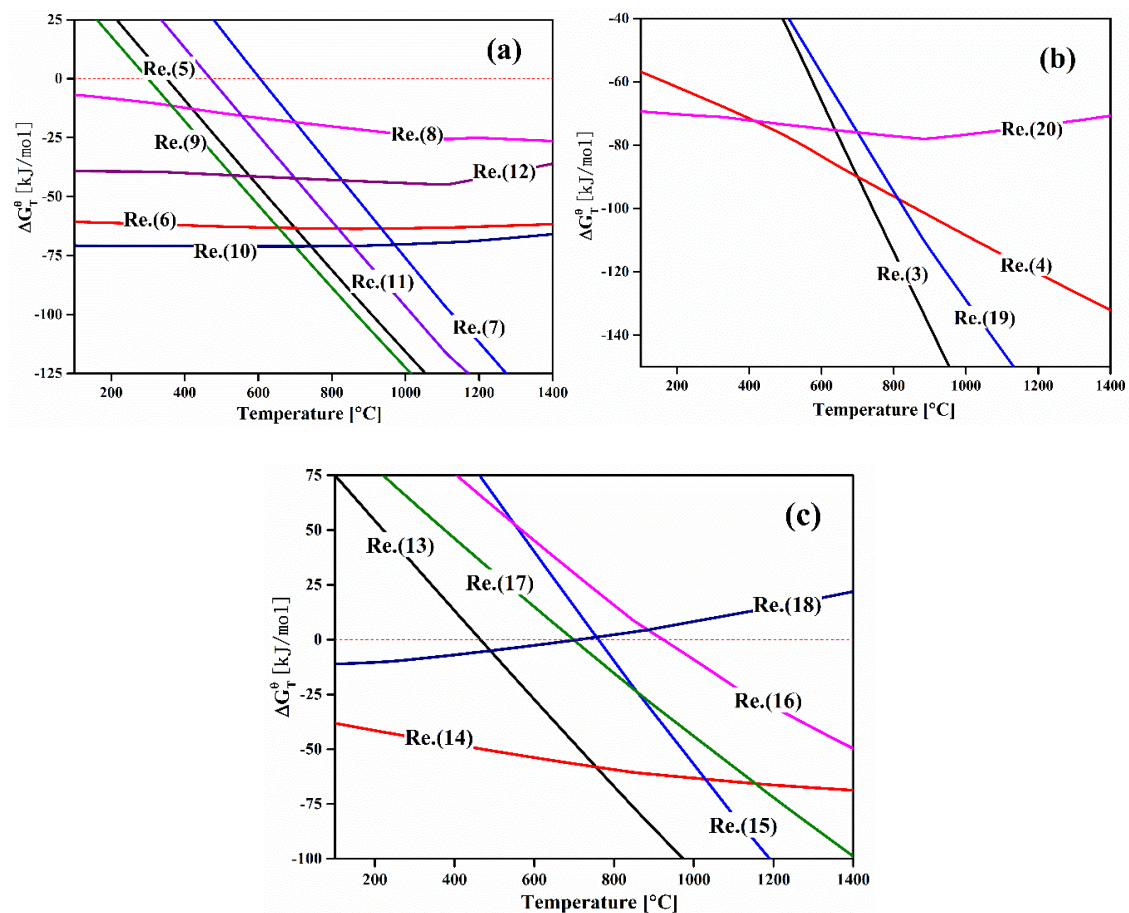

Figure 4. ΔG_T^θ-*T* diagram of Reactions (3)–(20). The data were obtained from HSC Chemistry 9.2.6 and its database [31]. (**a**) ΔG_T^θ-*T* diagram of Reactions (5)–(12); (**b**) ΔG_T^θ-*T* diagram of Reactions (3),(4),(19) and (20); (**c**) ΔG_T^θ-*T* diagram of Reactions (13)–(18).

4. Results and Discussion

4.1. Effect of Fe/SiO$_2$

The effect of Fe/SiO$_2$ on the direct Pb recovery and the sulfur-fixing rates was investigated in the range from Fe/SiO$_2$ = 0.65 to 1.3 (*w/w*), with a fixed conditions of W_{coke} = 10% $W_{\text{raw materials}}$, molten salt addition $W_{\text{Na}_2\text{CO}_3 + \text{Na}_2\text{SO}_4}$ = 18% $W_{\text{raw materials}}$ and molten salt composition $W_{\text{Na}_2\text{CO}_3}/W_{\text{Na}_2\text{SO}_4}$ = 0.3/0.7 (where *W* represents weight), CaO/SiO$_2$ = 0.3, smelting at 1200 °C for 2 h. The results are illustrated in Figure 5. It can be observed that the direct Pb recovery increased gradually with increasing Fe/SiO$_2$ and peaked at Fe/SiO$_2$ = 1.1 where 85.3% Pb was directly recovered. However, a steady declining trend was observed when the Fe/SiO$_2$ was above 1.1. Otherwise, the sulfur-fixing rate increased slowly from 89.5% to 95.5% as Fe/SiO$_2$ increased from 0.65 to 1.3, and reached a maximum sulfur-fixing rate of 96.7% at Fe/SiO$_2$ = 1.25. This can be explained by the fact that a large fraction of iron oxide in the slag promotes the sulfur-fixing reactions.

Figure 6 illustrates a liquidus surface diagram of the PbO-FeO-SiO$_2$-CaO-Na$_2$O system with fixed ratio of $W_{\text{Na}_2\text{O}}/W_{\text{SiO}_2}$ = 0.5 and $W_{\text{CaO}}/W_{\text{SiO}_2}$ = 1/3. It reveals that the temperature of liquid phase boundaries deceased with the increasing FeO fraction. This indicates that a suitable FeO addition decreases the melting point of the slag; at the same time, the viscosity and fluidity will also be improved. As a result, the reduction and settling environment of lead particles are improved. However, it is also

observed that excessive FeO fraction will also lead to a higher melt density and higher melting point in slag. It is unbeneficial to the settling and elimination of Pb droplets. At the same time, the blue liquidus lines gradually moved to PbO corner with the increasing FeO fraction. This indicates that the solubility of lead increase in the slag. Therefore, a moderate addition of iron helps to obtain a suitable FeO-SiO$_2$-CaO-Na$_2$O slag for effective lead recovery and sulfur-fixation.
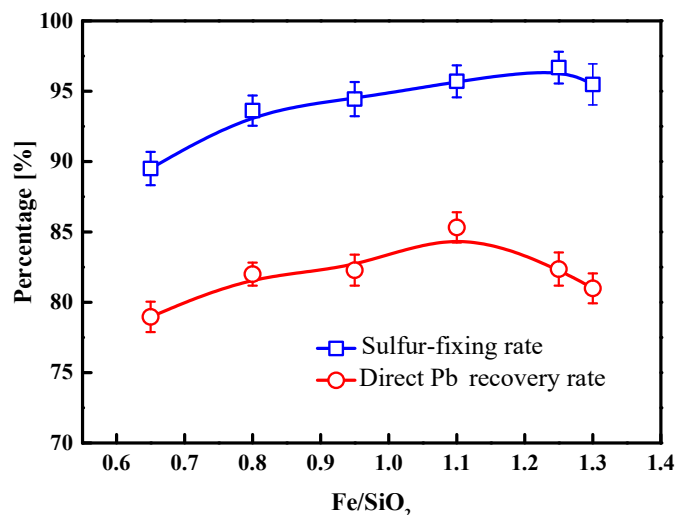

Figure 5. Effect of Fe/SiO$_2$ on the Pb recovery and sulfur-fixing efficiency. (W_{coke} = 10% $W_{raw\ materials}$, $W_{Na_2CO_3\ +\ Na_2SO_4}$ = 18% $W_{raw\ materials}$, $W_{Na_2CO_3}/W_{Na_2SO_4}$ = 0.3/0.7, CaO/SiO$_2$ = 0.3, 1200 °C, 2 h).
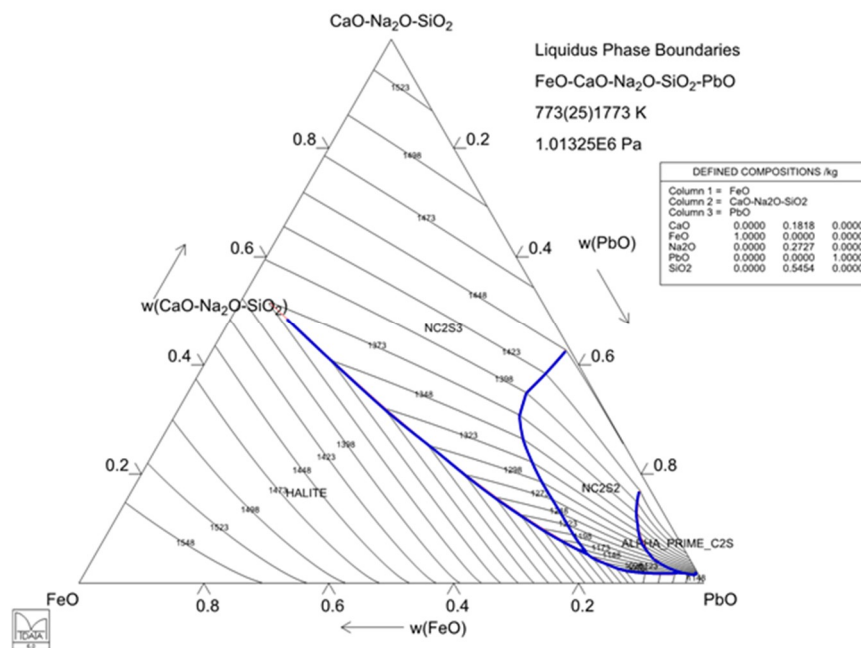
Figure 6. Liquidus contour diagram of the PbO-FeO-SiO$_2$-CaO-Na$_2$O system, the data was taken from MTDATA vers. 8.2 [32] MTOX database [33].

4.2. Effect of CaO/SiO$_2$ Ratio of the Slag

Figure 7 shows the effect of CaO/SiO$_2$ ratio of the silicate slag on the lead extraction and sulfur fixation. It is observed that the direct Pb recovery dropped sharply from 86.4% to 69.4% when CaO/SiO$_2$ was increased from 0.3 to 0.45. This indicates that the increasing CaO/SiO$_2$ was harmful to the settling of metallic lead. However, the change of CaO/SiO$_2$ had almost no effect on sulfur-fixing rate. It remained nearly constant in around 97%. Figure 8 illustrates a liquidus contour diagram of the

CaO-FeO-SiO$_2$-Na$_2$O system in fixed W_{Na_2O}/W_{SiO_2} ratio of 0.5. It also indicates that increasing addition of CaO will lead to an increase in melting point of the slag. As a result, the viscosity and fluidity of slag will also deteriorate. The Pb recovery showed a diminishing trend at higher CaO additions.
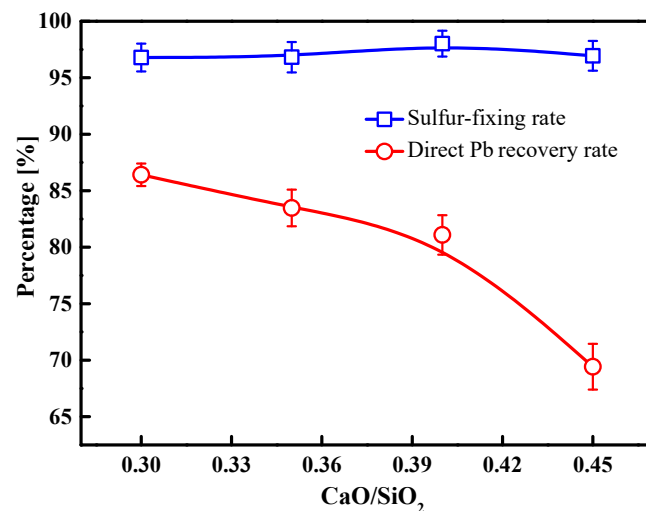

Figure 7. Effect of CaO/SiO$_2$ ratio on the direct Pb recovery and sulfur-fixing efficiency. ($W_{coke} = 10\% W_{raw\ materials}$, $W_{Na_2CO_3\ +\ Na_2SO_4} = 18\% W_{raw\ materials}$, $W_{Na_2CO_3}/W_{Na_2SO_4} = 0.3/0.7$, Fe/SiO$_2$ = 1.1, 1200 °C, 2 h).
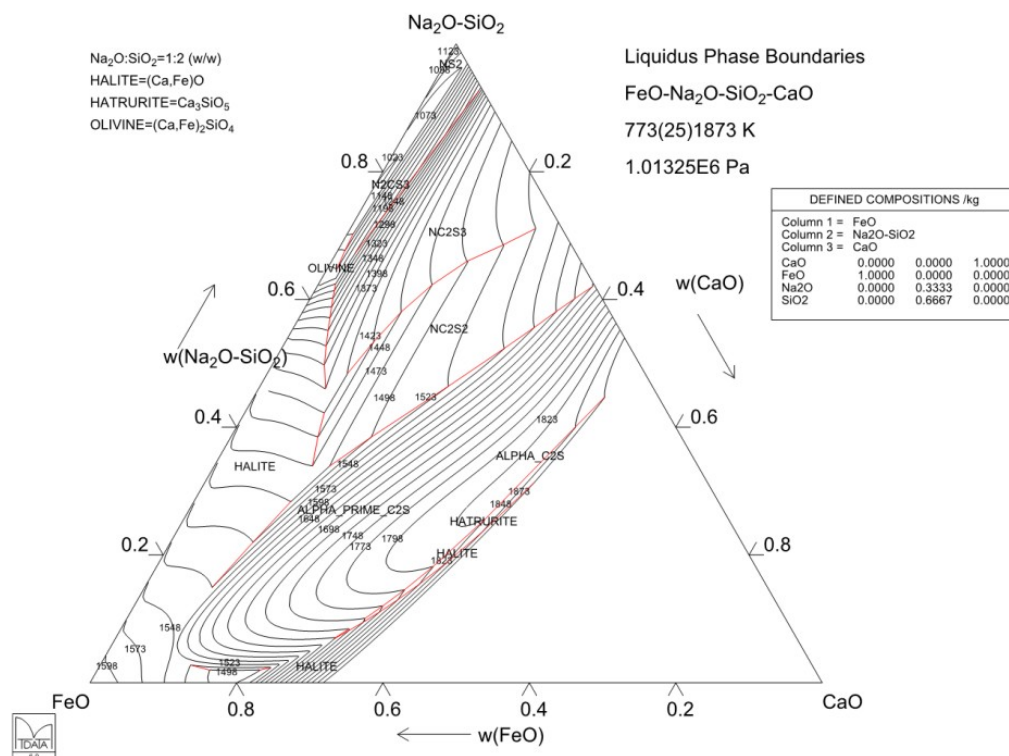
Figure 8. Liquidus contour diagram of the CaO-FeO-Na$_2$O-SiO$_2$ system with W_{Na_2O}/W_{SiO_2} = 0.5. The data was taken from MTDATA vers. 8.2 MTOX database.

4.3. Effect of $W_{Na_2CO_3}/W_{Na_2SO_4}$

The relationship between $W_{Na_2CO_3}/W_{Na_2SO_4}$ and Pb recovery and sulfur-fixing rates are presented in Figure 9. It can be seen that the direct Pb recovery increased steadily from 85.3% to 90.8% as the $W_{Na_2CO_3}/W_{Na_2SO_4}$ increased from 0.3/0.7 to 0.9/0.1. However, the sulfur-fixing rate was

constant on around 95.5%. Molten salt can simultaneously decrease the melting point, density, viscosity [34,35], and improve the fluidity of the slag [36]. Therefore, Na_2CO_3-Na_2SO_4 mixture can provide a flexible reaction medium and significantly promote the smelting reactions. Figure 10 illustrates the phase diagram of the binary Na_2CO_3-Na_2SO_4 system. It shows that the melting temperature of Na_2CO_3-Na_2SO_4 mixture decreases with increasing Na_2CO_3 fraction, and reaches the minimum in $W_{Na_2CO_3}/W_{Na_2SO_4}$ = 0.54/0.45. Therefore, with increasing $W_{Na_2CO_3}/W_{Na_2SO_4}$ ratio, the settling environment of lead particles was improved. More metallic Pb was settled and collected in crude lead.
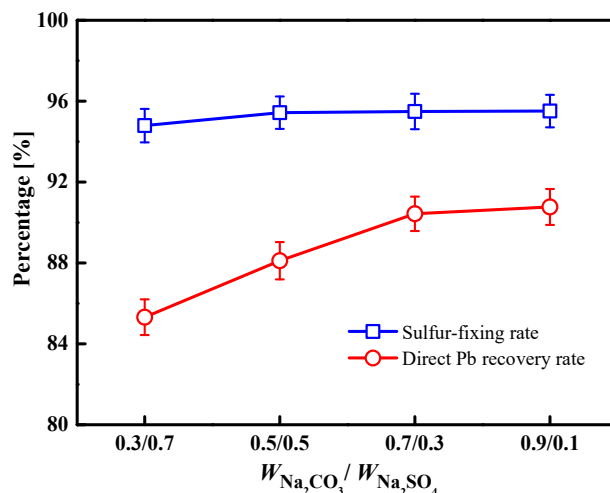

Figure 9. Effect of Na_2CO_3/Na_2SO_4 ratio on the Pb recovery and sulfur-fixing efficiency (W_{coke} = 10%$W_{raw\ materials}$, $W_{Na_2CO_3\ +\ Na_2SO_4}$ = 18%$W_{raw\ materials}$, Fe/SiO_2 = 1.1, CaO/SiO_2 = 0.3, 1200 °C, 2 h).
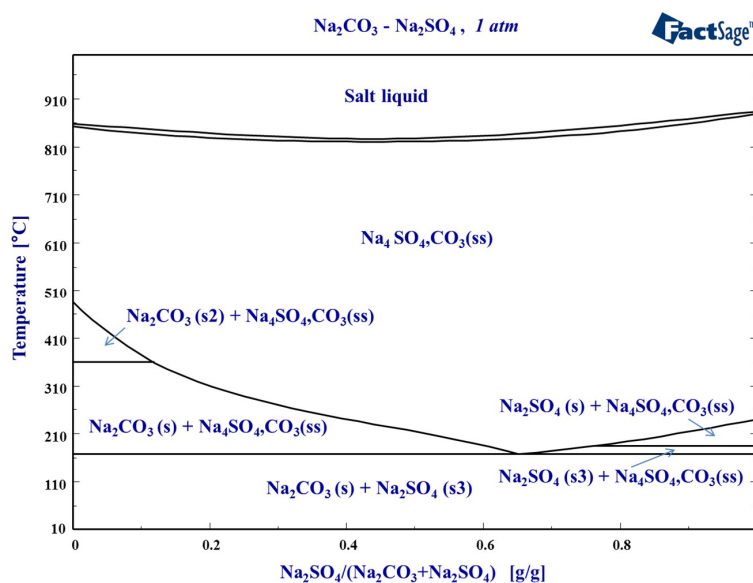

Figure 10. Phase diagram of the Na_2CO_3-Na_2SO_4 system; the data was taken from FactSage 7.2 and its FTsalt database [37].

4.4. Effect of Coke Addition

Figure 11 illustrates the effect of coke addition on the smelting yields. When coke dosage was increased from 5% to 25%, Pb extraction was found to increase from 81.3% to 91.5%, and it reached a maximum of 92.4% at 20% coke addition. The sulfur-fixing rate increased from 91.7% to 94.8%, and peaked at 97.2% with 15% coke addition. However, a small decrease of sulfur-fixation was observed when the coke addition was more than 15%. Strong reductive atmosphere was beneficial to the reduction and enrichment of lead. It was also intended to promote iron oxide reduction. More Fe_xO_y

was reduced to generate metallic Fe and then transferred into crude lead phase. Afterwards, iron oxide acting as sulfur-fixation agent correspondingly decreased. As a result, the slag composition was turned to a direction that was against the Pb recovery, as shown in Figure 6. Therefore, a slight decrease was observed in both the Pb recovery and sulfur-fixation beyond 15% coke addition.
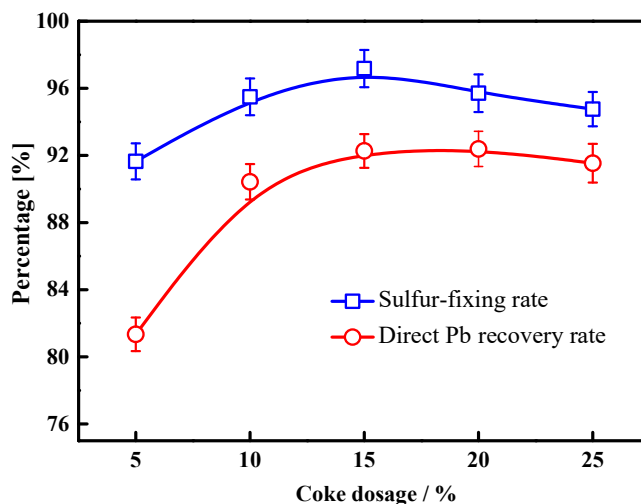
Figure 11. Effect of coke dosage on the Pb recovery and sulfur-fixing efficiency ($W_{\mathrm{Na_2CO_3 + Na_2SO_4}}$ = 18%$W_{\mathrm{Pb\ materials}}$, $W_{\mathrm{Na_2CO_3}}/W_{\mathrm{Na_2SO_4}}$ = 0.7/0.3, Fe/SiO$_2$ = 1.1, CaO/SiO$_2$ = 0.3, 1200 °C, 2 h).

4.5. Effect of Smelting Temperature

The direct Pb recovery and sulfur-fixing rates at different temperatures are shown in Figure 12. Below 1200 °C, Pb recovery and sulfur-fixing rates presented a sharp rising trend with increasing temperatures. The Pb recovery increased from 58.3% to 93.3% and sulfur-fixing rate increased at the same time from 75.9% to 96.2%. The phase diagram of the PbO-FeO-SiO$_2$-CaO-Na$_2$O system shown in Figure 6 also indicates that increasing temperature is beneficial to decrease the PbO content in the slag. However, direct Pb recovery steadily decreased when the temperature was higher than 1200 °C due to the intensified volatilization of metallic Pb, but sulfur-fixation continued to increase slightly. Therefore, a suitable smelting temperature was critical to achieve a high direct Pb recovery to the molten metal, and to avoid lead losses in the off-gas fumes.
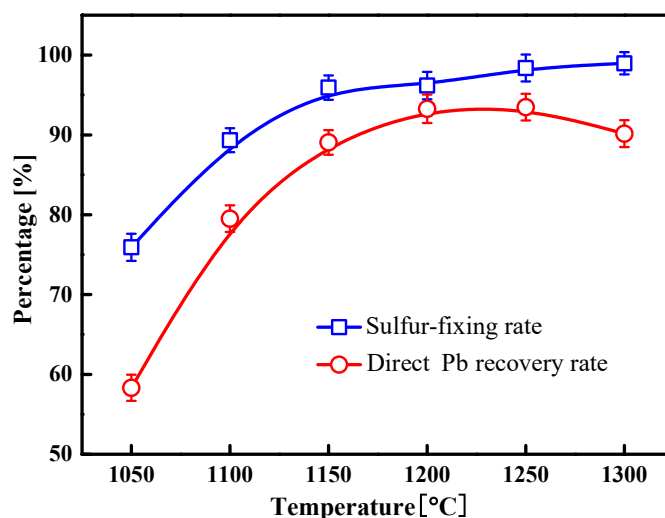
Figure 12. Effect of temperature on the Pb recovery and sulfur-fixing efficiency (W_{coke} = 15%$W_{\mathrm{Pb\ materials}}$, $W_{\mathrm{Na_2CO_3 + Na_2SO_4}}$ = 18%$W_{\mathrm{Pb\ materials}}$, $W_{\mathrm{Na_2CO_3}}/W_{\mathrm{Na_2SO_4}}$ = 0.7/0.3, Fe/SiO$_2$ = 1.1, CaO/SiO$_2$ = 0.3, 2 h).

4.6. Effect of Smelting Time

Figure 13 shows the effect of smelting time on the Pb recovery and sulfur-fixation. It illustrates that extending the smelting time can promote the recovery of Pb and sulfur fixation. 93.3% Pb and 97.5% sulfur were recovered and immobilized within 2 h of reaction. After 3 h, Pb recovery and sulfur-immobilization rates were 92.6% and 98.3%, respectively. This indicates 2 h reaction time was enough for the settling and enrichment of the Pb product in the bullion. The further extension of smelting time would lead to a gradual decline in Pb recovery due to volatilization of metallic Pb. When the smelting time was increased from 2 h to 3 h, the sulfur-fixing rate showed a slight increase from 97.5% to 98.3%. Considering the volatilization of Pb and energy consumption, the optimum smelting time was suggested to be around 2 h.
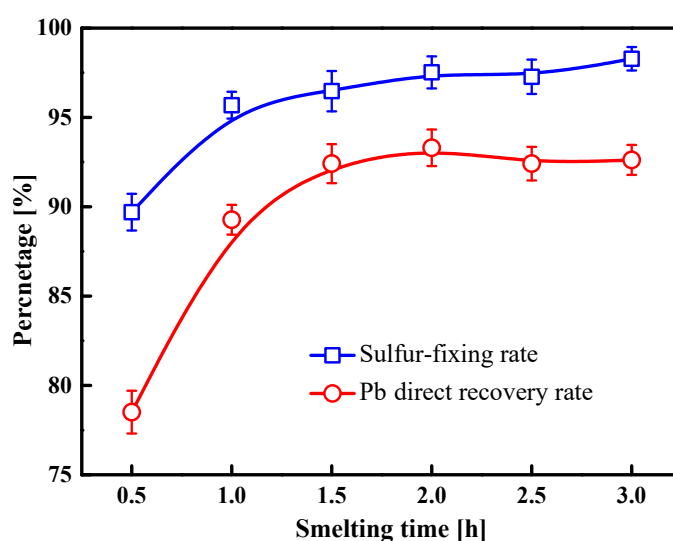

Figure 13. Effect of smelting time on the Pb recovery and sulfur-fixing efficiency (W_{coke} = 15% $W_{Pb\ materials}$, $W_{Na_2CO_3\ +\ Na_2SO_4}$ = 18% $W_{Pb\ materials}$, $W_{Na_2CO_3}/W_{Na_2SO_4}$ = 0.7/0.3, Fe/SiO$_2$ = 1.1, CaO/SiO$_2$ = 0.3, 1200 °C).

4.7. Bench-Pilot Experiments

Based on the above detailed experiments in the laboratory, the optimum processing conditions were obtained as: $W_{coke}/W_{raw\ materials}$ = 15%, $W_{Na_2CO_3\ +\ Na_2SO_4}$ = 18% $W_{raw\ materials}$, $W_{Na_2CO_3}/W_{Na_2SO_4}$ = 0.7/0.3, Fe/SiO$_2$ = 1.1, CaO/SiO$_2$ = 0.3, smelting temperature 1200 °C, and smelting time 2 h. These conditions were then applied to carry out two bench-pilot experiments with 200g Pb-bearing materials mixture. The chemical compositions of different products obtained, crude Pb, ferrous matte and slag, were presented in Table 3. It was found that lead concentrations in the ferrous matte and slag were below 2.4% and 0.7%, respectively. Purity of the crude lead was higher than 96.5%, and its main impurity was metallic Fe.

Table 3. Chemical compositions of smelting products in the bench-pilot experiments (wt.%).

No.	Crude Pb			Ferrous Matte					Slag						
	Pb	Fe	Ag *	Pb	Fe	S	Zn	Na	Pb	Fe	S	Zn	Na	CaO	SiO$_2$
1	96.06	2.12	821	2.54	48.80	24.07	2.36	7.47	0.61	23.01	4.21	1.51	8.65	8.59	27.30
2	97.02	1.72	845	2.30	50.19	24.51	3.30	6.94	0.72	24.58	3.07	1.83	8.24	8.97	28.71
AVG.	96.54	1.92	833	2.42	49.50	24.29	2.83	6.71	0.67	23.80	3.64	1.67	8.45	8.78	28.01

* g/t.

The optical macrograph and XRD results of smelting products are illustrated in Figure 14. It was observed that the product was separated to three layers: slag, ferrous matte, and crude lead. Slag floats on the surface of the ferrous matte, and metallic Pb subsides at the bottom due to their density differences, which guarantees a good separation and recovery during the smelting process. In addition, the main components in the solidified matte were FeS, $NaFeS_2$, and $Fe_2Zn_3S_5$. It indicated that sulfur was fixed in the matte in form of sulfide matte. A little entrained metallic Pb phase was also detected in it. The slag was a FeO-SiO_2-CaO-Na_2O quaternary and solidified as a vitreous slag system.
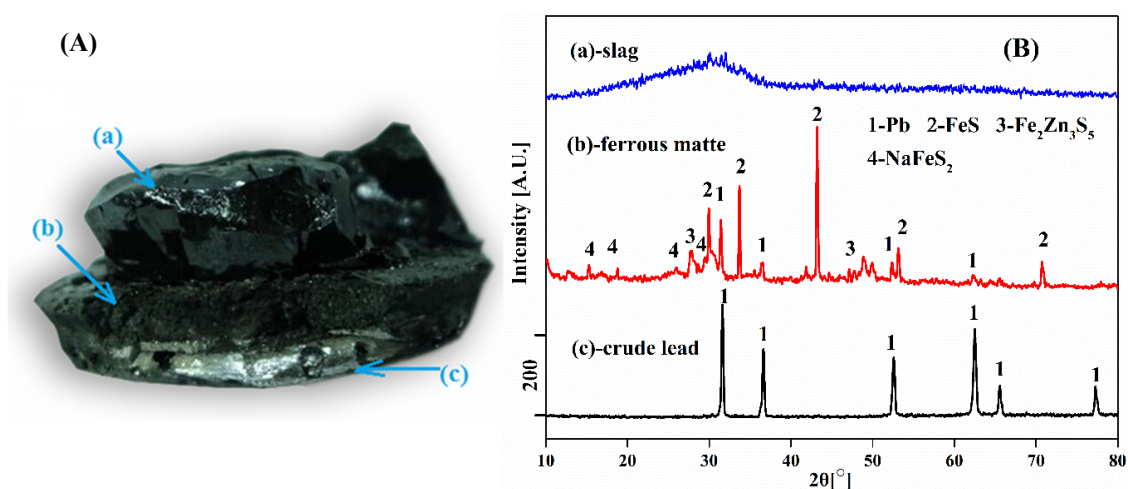

Figure 14. (**A**) Physical macrograph and (**B**) XRD patterns of the products in the bench-pilot experiments.

The distribution behaviors of Pb, Ag, Fe, and S in the bench-pilot experiments are summarized in Figure 15. As shown, 92.4% Pb could be directly enriched in the crude lead, and only 5.5% and 1.8% of Pb distributed into the ferrous matte and slag, respectively. 98.8% of Ag was also enriched in crude lead. 71.0% of iron was divided into ferrous matte as sulfide and the rest of 28.7% was in the FeO-SiO_2-CaO-Na_2O slag, respectively. Total sulfur-fixed rate was 98.6% to condensed phases, with 91.3% in matte, 7.3% in slag. At the same time, 0.2% sulfur was in crude lead. Only 1.2% distributed to the fume. Therefore, this novel reductive sulfur-fixing smelting process can significantly inhibit the generation of SO_2 and largely decrease the SO_2 emissions.
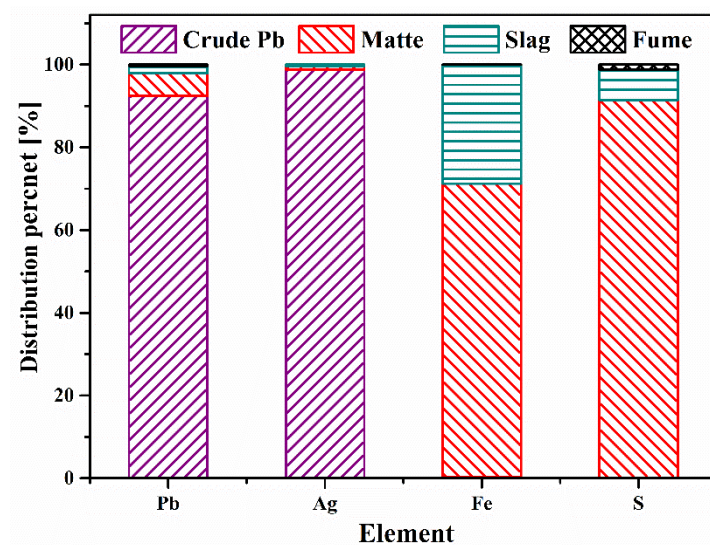

Figure 15. The distribution behaviors of Pb, Ag, Fe, and S in crude lead, ferrous matte, slag, and off-gas fume in the bench-pilot tests.

Recently, this novel Pb recycling process from polymetallic complex materials was industrially adopted [38] in several recycling plants in China, such as Guoda Nonferrous Metals Metallurgy Co., Ltd. [39] and Yongchang Precious Metals Co., Ltd. It has practically proved feasible. The industrial application results indicate that this process can be steadily executed on a continuous basis and offers advantages of low dust generation and high production capacity in currently available smelting furnaces. The operating expenditure was reduced significantly. The off-gas emissions met the relevant Chinese standards. Furthermore, the matte produced can be sold directly for sulfuric acid manufacture and regenerated as sulfur-fixing agent. The slag is harmless and can be used as a raw material for cement production after water-quenching and granulation. Otherwise, in addition to LAB paste recycling, it also can be used for treating antimony- [28,30], bismuth- [40], zinc- [41], and copper-containing [42] wastes and residues. Sb and Bi are enriched and recovered in the bullion. Zinc and copper are primarily distributed to the sulfide matte. Direct recoveries of the metals, i.e., yields without subsequent slag cleaning and matte processing, reach more than 90%, and the sulfur-fixing rate is generally higher than 95%.

5. Conclusions

Cleaner extraction of lead from complex polymetallic lead-containing wastes using reductive sulfur-fixing smelting process was fundamentally and experimentally confirmed to be feasible. The optimum smelting conditions were determined in this study as: $W_{coke} = 15\% W_{raw\ materials}$, $W_{Na_2CO_3}/W_{Na_2SO_4} = 0.7/0.3$, $Fe/SiO_2 = 1.1$, $CaO/SiO_2 = 0.3$, smelting temperature 1200 °C and smelting time 2 h. Under these conditions, three smelting products, crude lead, ferrous matte, and slag, were obtained. While 92.4% Pb was directly recovered as crude lead, 98.8% Ag was enriched in the crude lead. Lead concentration in the produced ferrous matte and slag were less than 2.4% and 0.7%, respectively. Purity of the crude lead was higher than 96.5%. Sulfur was fixed in the matte and slag as sulfide. The total sulfur-fixing rate was 98.3%, including 90.3% in the matte and 8.0% in the slag. Gaseous SO_2 generation and emissions could be essentially eliminated. This process is a promising high-efficiency technique that is cleaner and offers multiple application prospects in the fields of lead-, antimony-, bismuth-, zinc-, and copper-containing secondary materials, wastes, and residues recycling.

Author Contributions: Y.L. contributed to the works of literature search, figures, data collection, data analysis and writing—review and editing; S.Y. contributed to the conceptualization and supervising works; W.L. and Y.L. performed the experiments together, and W.L. wrote the original draft; J.H. and Y.W. contributed to the design of the work; J.S. contributed to the data analysis. Y.C., C.T., and A.J. played a contributor role of study design, data interpretation, and project administration; A.J. and P.T. contributed the work of writing—review and editing and final approval of the version to be published.

Conflicts of Interest: The authors declare no conflict of interest.

References

1. Lassin, A.; Piantone, P.; Burnol, A.; Bodénan, F.; Chateau, L.; Lerouge, C.; Crouzet, C.; Guyonnet, D.; Bailly, L. Reactivity of waste generated during lead recycling: An integrated study. *J. Hazard. Mater.* **2007**, *139*, 430. [CrossRef]

2. Ellis, T.W.; Mirza, A.H. The refining of secondary lead for use in advanced lead-acid batteries. *J. Power Sources* **2010**, *195*, 4525–4529. [CrossRef]

3.　Sahu, K.K.; Agrawal, A.; Pandey, B.D. Recent trends and current practices for secondary processing of zinc and lead. Part II: Zinc recovery from secondary sources. *Waste Manag. Res. J. Int. Solid Wastes Public Cleansing Assoc. Iswa* **2004**, *22*, 248–254. [CrossRef] [PubMed]

4.　Liu, J.Y.; Huang, S.J.; Sun, S.Y.; Ning, X.A.; He, R.Z.; Li, X.M.; Chen, T.; Luo, G.Q.; Xie, W.M.; Wang, Y.J. Effects of sulfur on lead partitioning during sludge incineration based on experiments and thermodynamic calculations. *Waste Manag.* **2015**, *38*, 336–348. [CrossRef] [PubMed]

5.　Nomura, Y.; Fujiwara, K.; Terada, A.; Nakai, S.; Hosomi, M. Prevention of lead leaching from fly ashes by mechanochemical treatment. *Waste Manag.* **2010**, *30*, 1290. [CrossRef] [PubMed]

6.　Okada, T.; Tojo, Y.; Tanaka, N.; Matsuto, T. Recovery of zinc and lead from fly ash from ash-melting and gasification-melting processes of MSW-comparison and applicability of chemical leaching methods. *Waste Manag.* **2007**, *27*, 69–80. [CrossRef] [PubMed]

7.　Li, Y.; Tang, C.; Chen, Y.; Yang, S.; Guo, L.; He, J.; Tang, M. *One-Step Extraction of Lead from Spent Lead-Acid Battery Paste via Reductive Sulfur-Fixing Smelting: Thermodynamic Analysis, 8th International Symposium on High-Temperature Metallurgical Processing*; Springer: Cham, Switzerland, 2017; pp. 767–777.

8.　Sun, Z.; Cao, H.; Zhang, X.; Lin, X.; Zheng, W.; Cao, G.; Sun, Y.; Zhang, Y. Spent lead-acid battery recycling in China—A review and sustainable analyses on mass flow of lead. *Waste Manag.* **2017**, *64*, 190–201. [CrossRef]

9.　Min, L.I.; Lin, Y.S. Lead pollution and its impact on human health in urban area. *Admin. Tech. Environ. Monitor.* **2006**, *5*, 6–10.

10.　Mishra, K.P.; Singh, V.K.; Rani, R.; Yadav, V.S.; Chandran, V.; Srivastava, S.P.; Seth, P.K. Effect of lead exposure on the immune response of some occupationally exposed individuals. *Toxicology* **2003**, *188*, 251–259. [CrossRef]

11.　Shen, H.; Forssberg, E. An overview of recovery of metals from slags. *Waste Manag.* **2003**, *23*, 933–949. [CrossRef]

12.　Zhang, W.; Yang, J.; Wu, X.; Hu, Y.; Yu, W.; Wang, J.; Dong, J.; Li, M.; Liang, S.; Hu, J. A critical review on secondary lead recycling technology and its prospect. *Renew. Sust. Energy Rev.* **2016**, *61*, 108–122. [CrossRef]

13.　He, D.; Yang, C.; Wu, Y.; Liu, X.; Xie, W.; Yang, J. $PbSO_4$ leaching in citric acid/sodium citrate solution and subsequent yielding lead citrate via controlled crystallization. *Minerals* **2017**, *7*, 93. [CrossRef]

14.　Ogundiran, M.B.; Nugteren, H.W.; Witkamp, G.J. Immobilisation of lead smelting slag within spent aluminate-fly ash based geopolymers. *J. Hazard. Mater.* **2013**, *S 248–249*, 29–36. [CrossRef] [PubMed]

15.　Albitar, M.; Ali, M.S.M.; Visintin, P.; Drechsler, M. Effect of granulated lead smelter slag on strength of fly ash-based geopolymer concrete. *Constr. Build. Mater.* **2015**, *83*, 128–135. [CrossRef]

16.　Vítková, M.; Ettler, V.; Šebek, O.; Mihaljevič, M.; Grygar, T.; Rohovec, J. The pH-dependent leaching of inorganic contaminants from secondary lead smelter fly ash. *J. Hazard. Mater.* **2009**, *167*, 427–433. [CrossRef] [PubMed]

17.　Şahin, M.; Erdem, M. Cleaning of high lead-bearing zinc leaching residue by recovery of lead with alkaline leaching. *Hydrometallurgy* **2015**, *153*, 170–178. [CrossRef]

18.　Barna, R.; Moszkowicz, P.; Gervais, C. Leaching assessment of road materials containing primary lead and zinc slags. *Waste Manag.* **2004**, *24*, 945–955. [CrossRef]

19.　Turan, M.D.; Altundoğan, H.S.; Tümen, F. Recovery of zinc and lead from zinc plant residue. *Hydrometallurgy* **2004**, *75*, 169–176. [CrossRef]

20.　Peng, R.; Ren, H.J.; Zhang, X.P. *Metallurgy of lead and zinc*; Science Press: Beijing, China, 2003; pp. 250–312.

21.　Liu, Q.; Tan, J.; Liu, C.Q.; Yin, Z.L.; Chen, Q.Y.; Zhou, L.; Xie, F.C.; Zhang, P.M. Thermodynamic study of metal sulfate decomposition process in bath smelting. *Chinese J. Nonferr. Metals* **2014**, *24*, 1629–1636.

22.　Street, S.; Brooks, G.; Reilly, L.; Worner, H.K. Environment and other bath smelting processes for treating organic and ferrous wastes. *JOM* **1998**, *50*, 43–47. [CrossRef]

23.　Pichler, C.; Antrekowitsch, J. Recycling of zinc- and lead-bearing residues with pyrolysis gas. *JOM* **2015**, *67*, 2038–2046. [CrossRef]

24.　Lin, D.; Qiu, K. Recycling of waste lead storage battery by vacuum methods. *Waste Manag.* **2011**, *31*, 1547–1552. [CrossRef] [PubMed]

25.　Ma, Y.; Qiu, K. Recovery of lead from lead paste in spent lead acid battery by hydrometallurgical desulfurization and vacuum thermal reduction. *Waste Manag.* **2015**, *40*, 151–156. [CrossRef] [PubMed]

26.　Smirnov, M. Direct smelting of lead at low temperature. *Nonferr. Metals* **1990**, *5*, 34–36.

27.　Margulis, E.V. Low temperature smelting of lead metallic scrap. *Erzmetall* **2000**, *53*, 85–89.

28. Li, Y.; Chen, Y.; Xue, H.; Tang, C.; Yang, S.; Tang, M. One-step extraction of antimony in low temperature from stibnite concentrate using iron oxide as sulfur-fixing agent. *Metals* **2016**, *6*, 153. [CrossRef]

29. He, D.W.; Yang, J.G.; Tang, C.B.; Chen, Y.M.; Tang, M.T. Separation of bismuth from a bismuth glance concentrate through a low-temperature smelting process. *Miner. Proc. Extrac. Metall. Rev.* **2013**, *34*, 73–80. [CrossRef]

30. Ye, L.G.; Tang, C.B.; Chen, Y.M.; Yang, S.H.; Yang, J.G.; Zhang, W.H. One-step extraction of antimony from low-grade stibnite in sodium carbonate–sodium chloride binary molten salt. *J. Cleaner Produc.* **2015**, *93*, 134–139. [CrossRef]

31. Roine, A. HSC chemistry 9.2.6. *Outotec Research Oy, Pori, Finland*. 2018. Available online: http://www.chemistry-software.com/ (accessed on 9 February 2018).

32. M.v., MTDATA ver. 8.2., NPL, Teddington, U.K. 2015. Available online: https://mtdata.com.au/ (accessed on 9 February 2018).

33. Gisby, J.; Taskinen, P.; Pihlasalo, J.; Li, Z.; Tyrer, M.; Pearce, J.; Avarmaa, K.; Björklund, P.; Davies, H.; Korpi, M.; et al. MTDATA and the prediction of phase equilibria in oxide systems: 30 years of industrial collaboration. *Metall. Mater. Trans. B* **2017**, *48*, 91–98. [CrossRef]

34. Ye, L.G.; Hu, Y.J.; Xia, Z.M.; Tang, C.B.; Chen, Y.M.; Tang, M.T. Solution behavior of ZnS and ZnO in eutectic Na_2CO_3–NaCl molten salt used for sb smelting. *J. Cent. South Univ.* **2017**, *24*, 1269–1274. [CrossRef]

35. Chen, Y.M.; Ye, L.G.; Tang, C.B.; Yang, S.H.; Tang, M.T.; Zhang, W.H. Solubility of sb in binary Na_2CO_3-NaCl molten salt. *Trans. Nonferrous Met. Soc. China* **2015**, *25*, 3146–3151. [CrossRef]

36. Ye, L.; Tang, C.; Chen, Y.; Yang, S.; Tang, M. The thermal physical properties and stability of the eutectic composition in a Na_2CO_3–NaCl binary system. *Thermochimica Acta* **2014**, *596*, 14–20. [CrossRef]

37. Bale, C.W.; Bélisle, E.; Chartrand, P.; Decterov, S.A.; Eriksson, G.; Gheribi, A.E.; Hack, K.; Jung, I.H.; Kang, Y.B.; Melançon, J.; et al. Factsage thermochemical software and databases, 2010–2016. *Calphad* **2016**, *54*, 35–53. [CrossRef]

38. Li, Y.; Yang, S.; Taskinen, P.; He, J.; Liao, F.; Zhu, R.; Chen, Y.; Tang, C.; Wang, Y.; Jokilaakso, A. Novel recycling process for lead-acid battery paste without SO_2 generation-reaction mechanism and industrial pilot campaign. *J. Clean. Produc.* **2019**, *217*, 162–172. [CrossRef]

39. Guoda Nonferrous Metals Smelting Co., L., Chenzhou, China. Company profile, 2009. Available online: http://www.czgdys.com.cn (accessed on 9 February 2018).

40. Lin, W.; Yang, S.; Tang, C.; Chen, Y.; Ye, L. One-step extraction of bismuth from bismuthinite in sodium carbonate–sodium chloride molten salt using ferric oxide as sulfur-fixing agent. *RSC Adv.* **2016**, *6*, 49717–49723. [CrossRef]

41. Ouyang, Z.; Ye, L.; Tang, C.; Chen, Y. Phase and morphology transformations in sulfur-fixing and reduction roasting of antimony sulfide. *Metals* **2019**, *9*, 79. [CrossRef]

42. Tang, L.; Tang, C.; Xiao, J.; Zeng, P.; Tang, M. A cleaner process for valuable metals recovery from hydrometallurgical zinc residue. *J. Clean. Produc.* **2018**, *201*, 764–773. [CrossRef]